Nanoscale

COMMUNICATION

Magnetization reversal and magnetic interactions in anisotropic Nd–Dy–Fe–Co–B/MgO/α-Fe disks and multilayers

Z. M. Dai,[a] W. Liu,*[a] X. T. Zhao,[a] T. T. Wang,[a] S. K. Li,[a] Yongsheng Yu, [iD] *[b] X. G. Zhao[a] and Z. D. Zhang[a]

We report on a field induced domain evolutionary procedure in the anisotropic Nd–Dy–Fe–Co–B/MgO/Fe multilayers by using first-order-reversal-curves and magnetic force microscopy. Different reversal behaviors and domain sizes are found in well coupled and decoupled multilayers by changing the thickness of the spacer layer. The competition between dipolar magnetostatic energy and Zeeman energy is evaluated by in-field observation throughout nucleation and annihilation processes. In addition, lithography-patterned arrays of soft Fe disks onto a continuous Nd–Dy–Fe–Co–B hard-magnetic layer are designed. By decreasing the applied field, it is found that magnetization orientations of the Fe disk and Nd–Dy–Fe–Co–B layer are aligned parallel. In the decoupled disk, although the out-of-plane magnetization orientations are observed, the orientation of the domains in the Fe disk is random. Furthermore, it is found that a stronger anisotropy of the Nd–Dy–Fe–Co–B layer decreases the interaction length. Our results provide a new understanding of anisotropic nanocomposite magnets with long-ranged magnetic interactions.

I. Introduction

Anisotropic nanocomposite permanent magnets have been extensively investigated since the discovery of remanence enhancement in $Fe_3B/Nd_2Fe_{14}B$ melt spun ribbons, which was first developed by Coehoorn *et al.* in 1988.[1] These nanocomposite magnets consisting of one magnetically hard component with high uniaxial magnetocrystalline anisotropy and one magnetically soft component with high saturation magnetization take advantage of the outstanding specific magnetic parameters of each phase. Theoretical considerations performed by Skomski and Coey show that anisotropic nanocomposite permanent magnets can have a maximum energy

density $(BH)_{max}$ as high as 1 MJ m^{-3}.[2] This theoretical value is considerably larger than those of currently existing magnets[3–5] and makes them possible next generation permanent magnets. However, it is difficult to prepare anisotropic nanocomposite permanent magnets due to the difficulties in controlling the formation and alignment of the hard-magnetic (HM) phase and diffusion between the hard- and soft-magnetic (SM) phases. Compared with bulk nanocomposite magnets, it is easier to control the nanostructure in thin films. In 2008, Cui *et al.* realized anisotropic nanocomposite multilayers by inserting a non-magnetic spacer layer to prevent diffusion between the SM and HM layers.[6,7] In this way, a $(BH)_{max}$ of 486 kJ m^{-3} was obtained in a Nd–Fe–B/Ta/FeCo multilayer film in the following experiment.[8] In previous work,[9] it was found that SM and HM layers were dominated by dipolar interactions and well coupled over a very long distance, which is several times larger than that of the Rudermann–Kittel–Kasuya–Yosida (RKKY) type of interaction[10–12] and the Heisenberg exchange interaction.

Knowledge of the magnetic structure is very important for understanding the nature of magnetism at the nanometer length scale and for the development of high-performance magnets.[13–16] In nanocomposite magnets, the process of magnetization reversal is very sensitive to phase composition, nanostructure, *etc.*[13,14] Although in bulk, due to the grain size in the nanometer scale hybrid structure, a large number of interfaces and the exchange coupling effect between grains, the mechanism of magnetization reversal becomes rather complicated and it is difficult to find intrinsic properties in the process of magnetization reversal.[15–18] Nanocomposite multilayers, which consist of independent soft- and hard-magnetic layers (SM/HM), present an advantage in controlling the competition of the surface- or interface-induced interactions. Therefore, it is desirable to further study the magnetic interactions *via* directly observing the domain structures in-field rather than making indirect conclusions.

In this paper, we investigate the domain structure and the magnetization processes in nanocomposite SM/HM multilayers by means of magnetic force microscopy (MFM)

[a]Shenyang National Laboratory for Materials Science, Institute of Metal Research, Chinese Academy of Sciences, Shenyang 110016, China. E-mail: wliu@imr.ac.cn
[b]MIIT Key Laboratory of Critical Materials Technology for New Energy Conversion and Storage, School of Chemistry and Chemical Engineering, Harbin Institute of Technology, Harbin, Heilongjiang 150001, China. E-mail: ysyu@hit.edu.cn

measurements in an applied magnetic field. The evolution of the domain structure in a perpendicular magnetic field was investigated in the demagnetization process after positive saturation. *In situ* observation was realized in patterned nano-composite SM/HM disks, which provided individual information in adjacent layers.

II. Experiments

The multilayers consist of Ta (30 nm)/Nd–Dy–Fe–Co–B (100 nm)/MgO (20/70 nm)/Fe (10 nm)/Ta (20 nm) and have been deposited by magnetron sputtering onto a Si (001) wafer. The deposition temperature and post-annealing temperature of the HM Nd–Dy–Fe–Co–B layers were set at 580 °C and 650 °C, respectively, to achieve a smooth interface. The 20 and 70 nm MgO spacers were chosen to achieve well-coupled and decoupled SM and HM phases, respectively. First-order-reversal-curves (FORCs) were obtained at room temperature with the field perpendicular to the film plane using a Quantum Design physical property measurement system (PPMS) with a vibrating-sample magnetometer (VSM) in a maximum field of 5 T. The local magnetization distribution was studied using the PPMS with a Scanning Probe Microscope (SPM). Topography scans were taken in tapping mode and the magnetic contrast was measured in an interleave scan with a lift

height of 80 nm. Periodic arrays of isolated Fe disks of 3 μm diameter were fabricated using standard lithography and lift-off techniques.

III. Results and discussions

The room temperature in-plane (IP) and out-of-plane (OOP) hysteresis loops of Nd–Dy–Fe–Co–B single layer, well-coupled and decoupled samples are shown in Fig. 1(a)–(c). Although a smooth hysteresis loop is presented in the OOP direction (Fig. 1(b)), a kink has appeared in the IP direction, which indicates that the interactions between SM and HM are changed with the measuring directions. Strong coupling leads to good squareness and higher remanence. In the demagnetiazation process, the interaction energy along the OOP direction, which can be estimated by the energy of magnetization reversal from remanence to the nucleation field, is given as

$$\sigma_i = \int_{M_N}^{M_r} H_{ex} dM$$

where M_r is the remanence, M_N is the magnetization at the nucleation field and H_{ex} is the external field.[19,20] When the SM and HM layers are well coupled, σ_i is about 3-11 mJ/m^{-2}, which is four times larger than that of the decoupled sample.
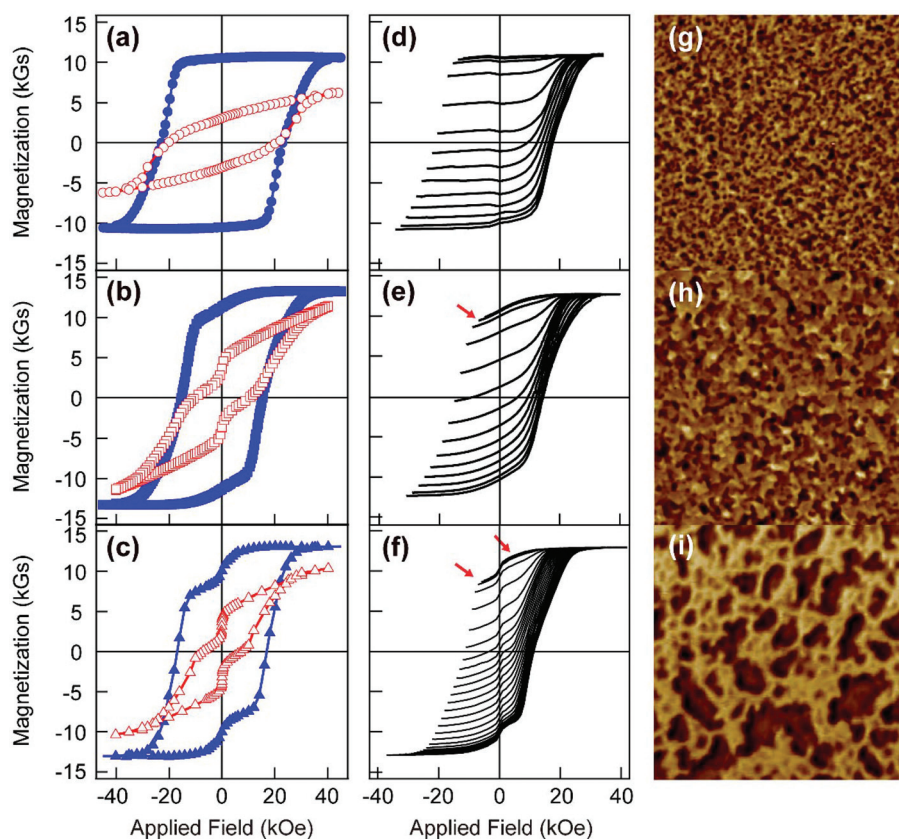

Fig. 1 The room temperature IP and OOP hysteresis loops (a)−(c), families of FORCs (d)−(f) and MFM images in the as-prepared state (g)−(i). For the Nd−Dy−Fe−Co−B single layer (a), (d) and (g), the well-coupled sample (b), (e) and (h), and the decoupled sample (c), (f) and (i), respectively.

The families of FORCs in the out-of-plane direction of the films are shown in Fig. 1(d)–(f). The acquisition of a FORC begins by saturating the system in a positive applied field. Then the applied field is decreased to a reversal field H_r, and the magnetization M is measured starting from H_r back to positive saturation. In Fig. 1(d), the Nd–Dy–Fe–Co–B single layer shows irreversible switching at a reversal field $H_r = -1.5$ T, where the FORCs deviate from the major loop after positive saturation of the samples.[21] Hereafter, nucleation of the domain starts, which indicates that the applied field does not bring the system back to the original state when the applied field returns. For the well-coupled film (20 nm MgO spacer), the same process of irreversible switching starts to occur at a reversal field $H_r = -0.7$ T. In Fig. 1(f), the decoupled film (70 nm MgO spacer) shows two separate irreversible switchings at $H_r = 0.4$ T and -0.6 T, respectively. The positive value of H_r is attributed to the SM phase, which indicates the initial nucleation before 0.4 T of applied field independently; as a result, the exchange-spring behavior between SM and HM magnets does not occur.

The as-prepared state is almost in a virgin state (thermally demagnetized). The MFM images of the Nd–Dy–Fe–Co–B single layer and the well-coupled and decoupled multilayer films are shown in Fig. 1(g)–(i), respectively. The scanned area is 10×10 μm^2. The yellow and brown contrast corresponds to out-of-plane up and down magnetizations, respectively. The image of the Nd–Dy–Fe–Co–B single layer (Fig. 1(g)) is characterized by a stripe domain with a magnetization oriented preferentially out-of-plane. The average domain width is 90 nm, which is a little larger than the grain size (60 nm). This phenomenon indicates the existence of interaction domains, but the magnetic coupling between grains is weak.[22,23] The size of the stripe domains extends when a 10 nm SM Fe layer and a 20 nm MgO spacer layer are added (well-coupled sample, Fig. 1(h)). This indicates that the easy direction of magnetization may slightly tilt away, but still mainly out-of-plane. When the spacer layer increases to 70 nm, the MFM image of the decoupled film (Fig. 1(i)) presents a quite different domain pattern from those shown in Fig. 1(g) and (h). A micron-sized domain with clear light and dark contrast is observed in the pattern. In addition to the micron-sized domain, small labyrinth stripe domains are also distributed in the pattern. This phenomenon of the two different domains coexisting in one pattern can be considered as characteristic of decoupled phases.[24]

In order to understand the behavior of domains at a specific field value, the applied magnetic field was applied perpendicular to the film during the measurement of the MFM images. In Fig. 2, the domain patterns of the well-coupled sample were obtained in the same surface region, as shown in Fig. 2(a). In Fig. 2(b)–(i), the applied field is continuously decreased from the positive saturation, where the yellow and blue colors correspond to out-of-plane up and down magnetizations, respectively. When the applied field is between 1 T to 0.1 T, as shown in Fig. 2(b) and (c), a nanosized stripe structure of the domains is observed. Upon decreasing the field,
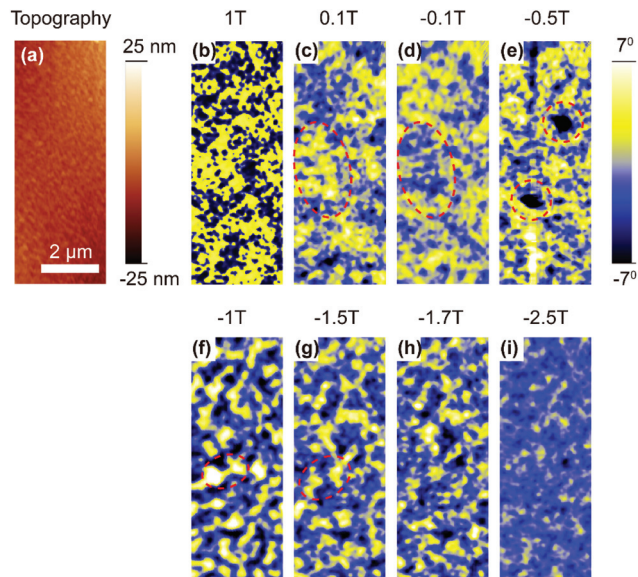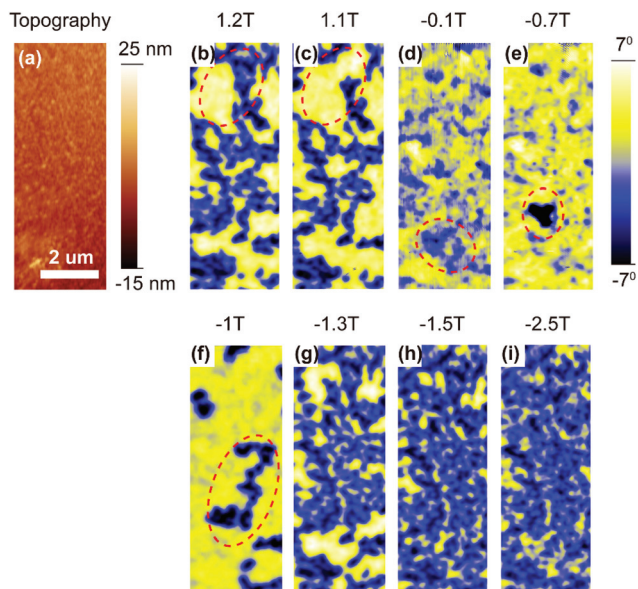

Fig. 2 MFM images of the well-coupled sample. The AFM topography (a) and the MFM images scanned at 1 T (b), 0.1 T (c), −0.1 T (d), −0.5 T (e), −1 T (f), −1.5 T (g), −1.7 T (h), and −3 T (i). All MFM images are obtained from the same area.

the domains parallel to the field weaken and reverse to the opposite direction as marked by the red ellipses in Fig. 2(c) and (d). When the applied field decreases to −0.5 T, near the irreversible switching field, new domains begin to nucleate, as marked by the red ellipses in Fig. 2(e). The new domains propagate and the residual domains are being annihilated. It can be seen from Fig. 2(f) that the domains have become larger at −1 T. When the applied field reaches −1.5 T, the magnetization follows the major loop, and the domains begin to annihilate gradually (see the red ellipses in Fig. 2(f) and (g)). Finally, at −2.5 T, the blue color covers most of the image (Fig. 2(i)), which indicates that the magnetization of the domains is nearly fully aligned.

Compared with the results on the well-coupled sample, the behavior of the decoupled sample can be divided into two separated nucleation processes. The first nucleation process begins before the applied field is decreased to 1.2 T. In Fig. 3(b) and (c), the micron-sized domains are marked with yellow and blue colors, while weak signs of nanosize domains are distributed between these patterns. The propagation process of the micron-sized domains is marked in the red ellipses at 1.2 T and 1.1 T. When the field decreases to −0.1 T (Fig. 3(d)), the domains begin to switch and annihilate. Nucleation of new domains occurs at −0.7 T (Fig. 3(e)). The new domains continuously propagate (see Fig. 3(f) and (g)) until the applied field is near coercivity (see Fig. 3(h) and (i)), where the annihilation process starts to occur.

In a simplistic consideration, the domain pattern reflects the competition between dipolar magnetostatic energy, Zeeman energy and domain wall energy. Based on the micromagnetic theory,[25,26] ferromagnetic multilayers with perpendicular magnetic anisotropy (PMA) always present stripe

Fig. 3 MFM images of the decoupled sample. The AFM topography (a) and the MFM images scanned at 1.2 T (b), 1.1 T (c), −0.1 T (d), −0.7 T (e), −1 T (f), −1.3 T (g), −1.5 T (h), and −2.5 T (i). All MFM images are obtained from the same area.

domains. Assuming the stripe period $D = d_{up} + d_{down}$ and the dimensionless parameter $q = (d_{up} - d_{down})/D$, where d_{up} and d_{down} are up and down domain widths, respectively, the energy density of a stripe domain can be written in the following form:[27,28]

$$w_s = 8\pi M^2 \frac{l_c}{D} - HMq + 2\pi M^2 \tilde{N}(D, q)$$

Here $l_c = \sigma/4\pi M^2$ is the characteristic length, defined by the ratio of wall-energy density σ and the magnetostatic energy

density $2\pi M^2$. The first term describes the domain wall energy density of the stripe domain pattern. The second term is the Zeeman term. It indicates that by increasing the external magnetic field, the domains which are aligned parallel to the field grow while the oppositely aligned domains get smaller. And the last term is associated with the dipolar magnetostatic interactions between pairs of the "charged" planes bounding the layers. $\tilde{N}(D, q)$ is an effective demagnetizing factor. Generally, the domain wall energy density increases with decreasing domain size; thus a strong dipolar interaction favors smaller domains.

It should be noted that without the HM layer, the magnetization of the SM thin film is aligned in-plane and there should be no stray field detected by MFM technology. But in both the well-coupled and decoupled nanocomposite multilayers, the out-of-plane magnetization is shown at the surface of the SM layer. It is concluded that although the domains of the SM layer are not aligned parallel with the coherent HM layers in a decoupled multilayer, a small angle between the moments of SM and HM layers forms due to the existence of the weak dipolar interactions between the SM and HM layers. Therefore, the magnetization of the SM layer contributes to the domains that are out of plane.

To investigate the magnetization reversal behavior between adjacent layers, patterned micron-size disk arrays were prepared. The lithography-patterned arrays of soft Fe disks onto a continuous Nd−Dy−Fe−Co−B hard-magnetic layer are shown in Fig. 4(a) and (b). The diameter of the disks is 3 μm and the distance between the centres of two adjacent disks is larger than 4 μm, which makes sure that there is no interaction between the disks. The results for the well-coupled and decoupled SM disks are shown in Fig. 4(c) and (d) at different applied fields. At 1.2 T, in both Fig. 4(c) and (d), the MFM image exhibits a different contrast between the surface of the Fe disk and the surrounding Nd−Dy−Fe−Co−B film. Here, the yellow and blue
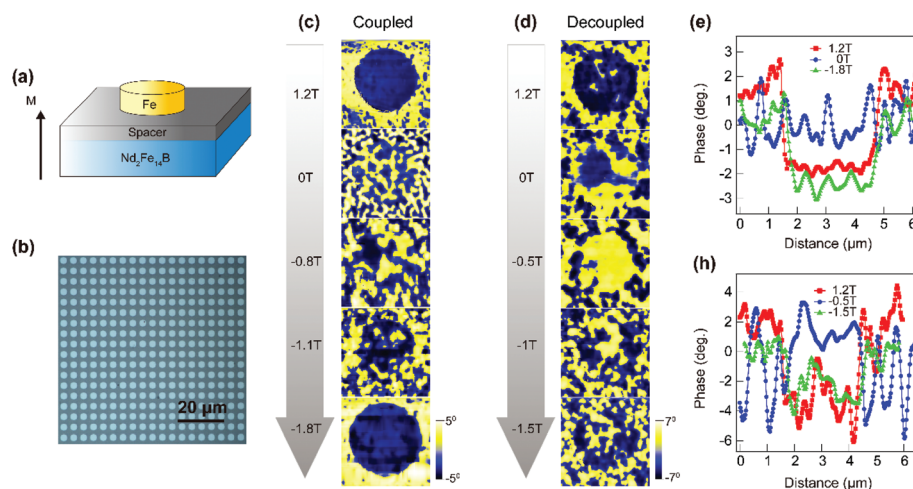
Fig. 4 The MFM images of the micron-sized SM disk. (a) Schematic illustration of lithography-patterned arrays of soft Fe disks onto a continuous Nd−Dy−Fe−Co−B hard-magnetic layer, and the well-coupled and decoupled structures are tuned by inserting a critical thickness of the spacer layer. (b) Optical image of the disk array prepared by lithography technology. (c) and (d) The in-field MFM images of the well-coupled and decoupled disks, respectively. (e) and (f) Line profiles extracted from MFM images shown in (c) and (d), respectively.

colors represent a relative phase intensity between the SM disk and HM layer. Thus, the line profiles (Fig. 4(e) and (f)) extracted from this applied field show opposite phase degrees along the Fe disk surface with the lower Nd–Dy–Fe–Co–B layer. As the MFM tip can only detect external stray fields, the large contrast of the phase signal may be associated with the different magnetization of the Fe-disk surface and the Nd–Dy–Fe–Co–B film.[29] Upon decreasing the applied field, in the well-coupled disk, the rim of the Fe disk becomes blurry in the remanent magnetization state and the ferromagnetic labyrinth stripe domains at the edge of disk are aligned continuously. This indicates that the magnetizations of the SM disk and adjacent HM layer are parallel, which is favored by strong dipolar fields. In addition, the signal intensities of SM and HM layers converge to the same level, as shown in Fig. 4(e). For a decoupled disk, a clear rim with incoherent orientation of the magnetization between the Fe disk and Nd–Dy–Fe–Co–B single layer is observed. Unlike the PMA antiferromagnetic multilayer, in which the magnetization of adjacent layers is antiparallel,[25] the magnetization orientation of the micron-sized domain in a decoupled disk is random. Upon increasing the field along the negative direction, the different nucleation behaviors of the well-coupled and decoupled disks are observed. In Fig. 4(c), the nucleation process occurs on the Fe disk and the Nd–Dy–Fe–Co–B layer nearly at the same time at −0.8 T. Next, the propagation and annihilation processes are presented at −1.1 T and −1.8 T, respectively. Finally, a clear negative phase signal appears again on the Fe disk. However, in the decoupled disk, the domains of the Fe disk propagate and the magnetization is nearly fully aligned at −0.5 T, while nucleation initially starts in the Nd–Dy–Fe–Co–B layer. We also measured other disks and the same result was achieved. In addition, it is found that the phase signal intensity of the Nd–Dy–Fe–Co–B layer is much larger than that in the Fe disk, as shown in Fig. 4(f).

Because the anisotropy of the Nd–Dy–Fe–Co–B permanent magnets is very sensitive to temperature, an *in situ* observation is presented at 160 K in the remanent magnetization state (Fig. 5(a) and (b)) to make clear the influence of the anisotropy on the interactions between the SM and HM phases. The

domain size of the Fe surface increases in comparison with the pattern at 300 K and 0 T, while the domain size of the Nd–Dy–Fe–Co–B film slightly decreases. This indicates that the effective interaction length becomes shorter when the anisotropy of the HM phase increases. For the decoupled disk, the domains of the Fe disk show a negative phase signal, which is opposite to the domains in the remanent magnetization state at 300 K in Fig. 5(b). This may indicate that the domains have not yet begun to switch.

IV. Conclusion

In conclusion, the dipolar interactions of SM and HM nanocomposite multilayers have been investigated by comparing the results of the well-coupled and decoupled samples. The differences of nucleation, propagation, switching, annihilation, and re-nucleation in well-coupled and decoupled samples have been investigated during the demagnetization process by decreasing the external applied field. By coupling with dipolar interactions, the well-coupled nanocomposite multilayer behaves in a unitary manner. The competition between the domain wall energy, Zeeman energy and dipolar magnetostatic energy has been discussed based on micromagnetic theory. It is concluded that a strong dipolar interaction between the SM and HM layers favors smaller domains. A micron-sized nanocomposite structure consisting of the soft Fe disks and the continuous Nd–Dy–Fe–Co–B film are manipulated by lithography. The Fe disks coupled with the Nd–Dy–Fe–Co–B film exhibit a coherent magnetization reversal. While the decoupled disk magnetization of the SM/HM layers is independent and nucleation initially starts from the Nd–Dy–Fe–Co–B layer at a negative descending field. Furthermore, it is found that a strong anisotropy of the Nd–Dy–Fe–Co–B layer decreases the interaction length. These results provide a microscopic understanding of magnetization reversal in the long-ranged dipolar interactions between soft- and hard-magnetic phases.

Acknowledgements

Fig. 5 MFM images of the well-coupled and decoupled disks at 160 K, respectively.

References

1 R. Coehoorn, D. B. de Mooij and C. de Waard, *J. Magn. Magn. Mater.*, 1989, **80**, 101–104.

2 R. Skomski and J. M. D. Coey, *Phys. Rev. B: Condens. Matter*, 1993, **48**, 15812–15816.

3 E. F. Kneller and R. Hawig, *IEEE Trans. Magn.*, 1991, **27**, 3588–3600.

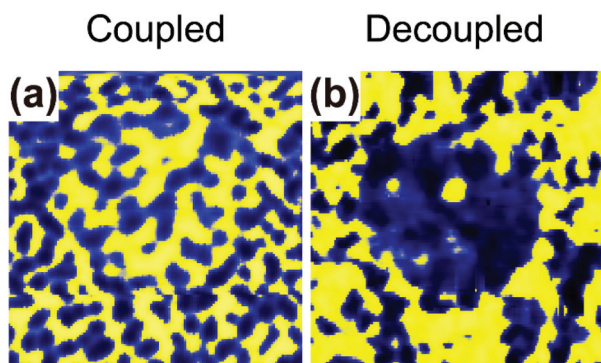4 Y. Kaneko, F. Kuniyoshi and N. Ishigaki, *J. Alloys Compd.*, 2006, **408**, 1344–1349.

5 G. C. Hadjipanayis and A. Kim, *J. Appl. Phys.*, 1988, **63**, 3310.

6 W. B. Cui, S. J. Zheng, W. Liu, X. L. Ma, F. Yang, Q. Yao, X. G. Zhao and Z. D. Zhang, *J. Appl. Phys.*, 2008, **104**, 053903.

7 W. B. Cui, W. Liu, W. J. Gong, X. H. Liu, S. Guo, F. Yang, Z. H. Wang and Z. D. Zhang, *J. Appl. Phys.*, 2012, **109**, 07B503.

8 W. B. Cui, Y. K. Takahashi and K. Hono, *Adv. Mater.*, 2012, **24**, 6530; W. B. Cui, Y. K. Takahashi and K. Hono, *Adv. Mater.*, 2013, **25**, 1966.

9 Z. M. Dai, W. Liu, X. T. Zhao, Z. Han, D. Kim, C. J. Choi and Z. D. Zhang, *J. Appl. Phys.*, 2016, **120**, 163906.

10 S. S. P. Parkin, N. More and K. P. Roche, *Phys. Rev. Lett.*, 1990, **64**, 2304–2308.

11 J. C. Slonczewski, *Phys. Rev. B: Condens. Matter*, 1989, **39**, 6995.

12 S. N. Okuno and K. Inomata, *Phys. Rev. Lett.*, 1994, **72**, 1553.

13 W. Szmaja, J. Grobelny, M. Cichomski, S. Hirosawa and Y. Shigemoto, *Acta Mater.*, 2011, **59**, 531.

14 H. Kronmüller, K.-D. Durst and M. Sagawa, *J. Magn. Magn. Mater.*, 1988, **74**, 291.

15 D. Goll, M. Seeger and H. Kronmüller, *J. Magn. Magn. Mater.*, 1998, **185**, 49.

16 H. W. Zhang, T. Y. Zhao, C. B. Rong, S. Y. Zhang, B. S. Han and B. G. Shen, *J. Magn. Magn. Mater.*, 2003, **267**, 224.

17 Z. B. Li, M. Zhang, B. G. Shen and J. R. Sun, *Appl. Phys. Lett.*, 2013, **102**, 102405.

18 G. P. Zhao, X. L. Wang, C. Yang, L. H. Xie and G. Zhou, *J. Appl. Phys.*, 2007, **101**, 09K102.

19 W. B. Cui, H. Sepehri-Amin, Y. K. Takahashi and K. Hono, *Acta Mater.*, 2015, **84**, 405–407.

20 D. Ogawa, K. Koike and H. Kato, *J. Korean Phys. Soc.*, 2013, **63**, 489–492.

21 C. R. Pike, C. A. Ross, R. T. Scalettar and G. Zimanyi, *Phys. Rev. B: Condens. Matter*, 2005, **71**, 134407.

22 D. J. Craik and E. D. Isaac, *Proc. Phys. Soc.*, 1960, **76**, 160–162.

23 J. D. Livingston, *J. Appl. Phys.*, 1985, **57**, 4137–4139.

24 O. Hellwig, A. Berger and E. E. Fullerton, *Phys. Rev. B: Condens. Matter*, 2007, **75**, 134416.

25 O. Hellwig, A. Berger, J. B. Kortright and E. E. Fullerton, *J. Magn. Magn. Mater.*, 2007, **319**, 13.

26 C. Bran, A. B. Butenko, N. S. Kiselev, U. Wolff, L. Schultz, O. Hellwig, U. K. Rössler, A. N. Bogdanov and V. Neu, *Phys. Rev. B: Condens. Matter*, 2009, **79**, 024430.

27 V. Neu, S. Melcher, U. Hannemann, S. Fähler and L. Schultz, *Phys. Rev. B: Condens. Matter*, 2004, **70**, 144418.

28 N. S. Kiselev, I. E. Dragunov, V. Neu, U. K. Rößler and A. N. Bogdanov, *J. Appl. Phys.*, 2008, **103**, 043907.

29 M. Labrune and L. Belliard, *Phys. Status Solidi A*, 1999, **174**, 483.